Electronic Supplementary Information (ESI) for

Syntheses, Gas Adsorption, and Sensing Properties of Solvent Controlled Zn(II) *Pseudo*-Supramolecular Isomers and Pb(II) Supramolecular Isomers

Jiang Wang[a], Lingling Gao[a], Jie Zhang[a], Li Zhao[a], Xiaoqing Wang[a], Xiaoyan Niu[a], Liming Fan[a*], and Tuoping Hu[a*]

Department of Chemistry, College of Science, North University of China, Taiyuan 030051, China.

E-mail: limingfan@nuc.edu.cn; hutuopingsx@126.com.

Structural Description of $[Zn(BTA)]_n$ (2)

Complex **2** crystallizes in triclinic space group *P*-1, the asymmetric unit contains one crystallographically independent Zn^{II} ion and two halves of BTA^{2-} ligands (Figure 1c). Each Zn^{II} ion is surrounded by two oxygen atoms (O1A and O3) and two nitrogen atoms (N2 and N3B) from four BTA^{2-} ligands, leaving a distorted $\{ZnO_2N_2\}$ tetrahedron geometry with τ4=0.85. The Zn-O bond lengths are 1.965(3) Å and 2.001(3) Å, the Zn-N bond lengths are 1.991(3) Å and 1.998(5) Å, respectively.

For **2**, the BTA^{2-} ligands adopt $(\kappa^1\text{-}\kappa^0)\text{-}\kappa^1\text{-}(\kappa^1\text{-}\kappa^0)\text{-}\kappa^1\text{-}\mu_4$ coordination mode (Mode I, Scheme 1) to connect Zn^{II} ions forming a 3D framework with the 1D channels (13.390 Å×10.617 Å). The porosity of **2** is 30.6% (275.2Å^3 out of 897.8 Å^3). The dihedral angles between phenyl ring and imidazolyl rings are 79.47° and 47.67° in the ligand of complex **2**.

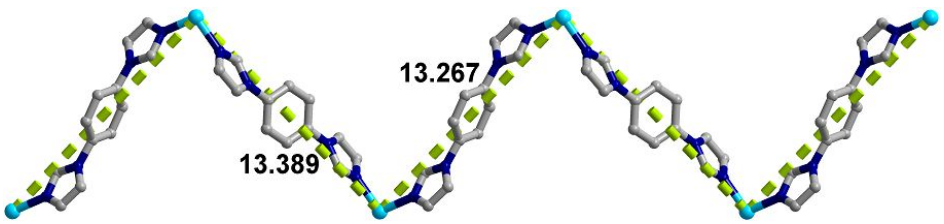

Figure S1. The 1D $[Zn(bib)]_n$ chain in **1**.

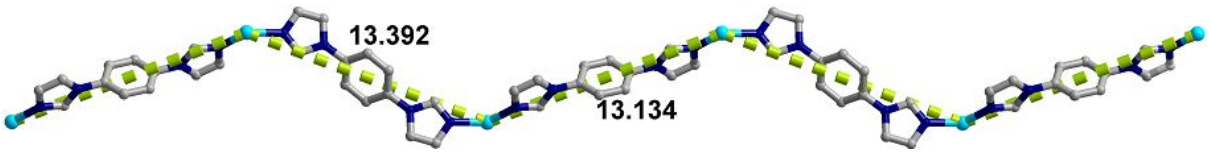

Figure S2. The 1D $[Zn(bib)]_n$ chain in **2**.

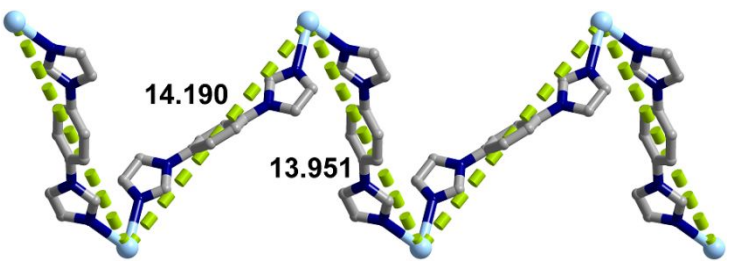

Figure S3. The 1D $[Pb(bib)]_n$ chain in **3**.

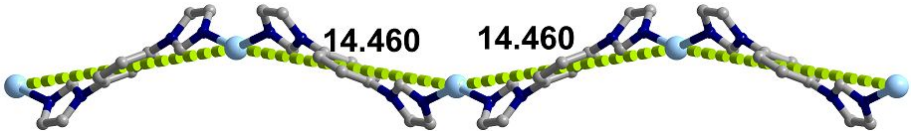

Figure S4. The 1D $[Pb(bib)]_n$ chain in **4**.

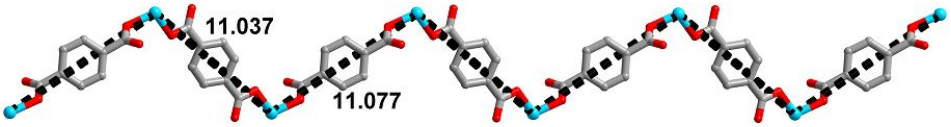

Figure S5. The 1D $[Zn(TPA)]_n$ chain in **1**.

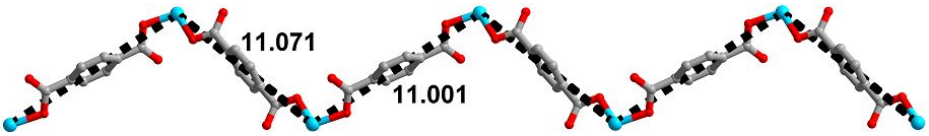

Figure S6. The 1D $[Zn(TPA)]_n$ chain in **2**.

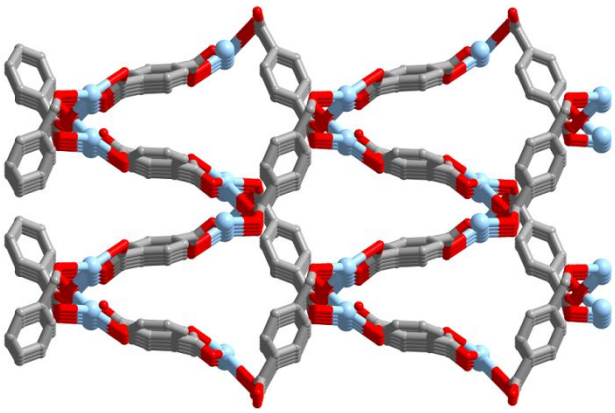

Figure S7. The 3D $[Pb(TPA)]_n$ network in **3**.

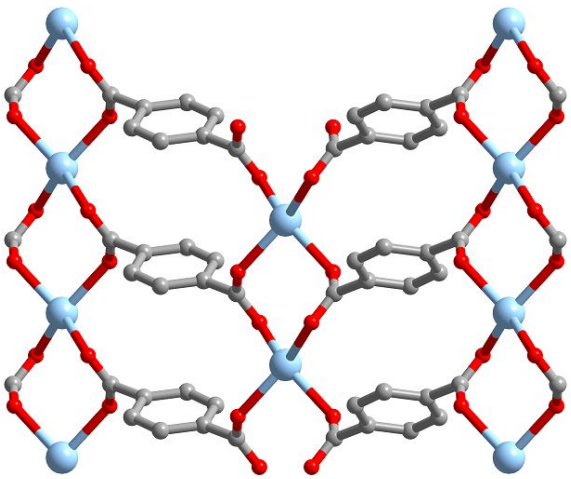

Figure S8. The 2D $[Pb(TPA)]_n$ sheet in **4**.

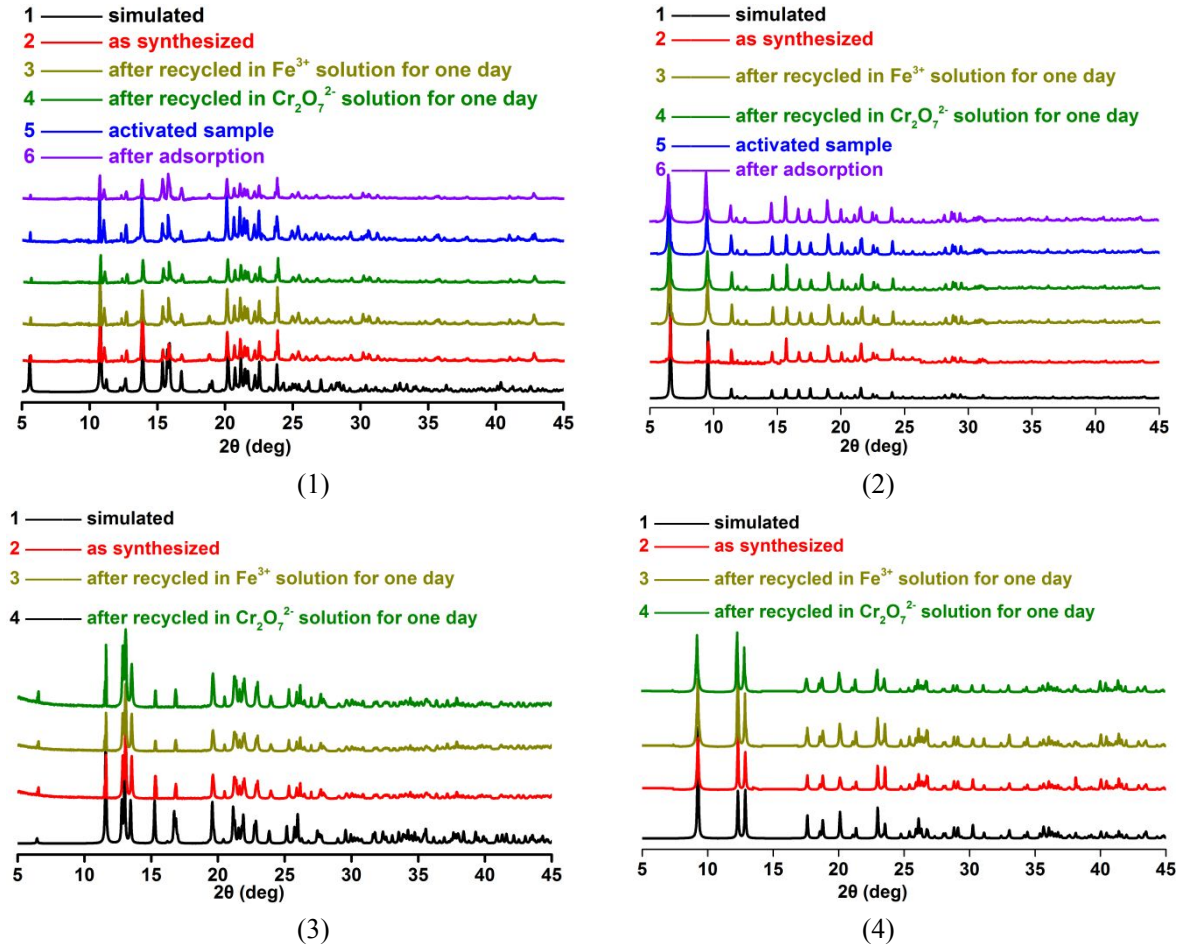

Figure S9. PXRD patterns of **1-4**.

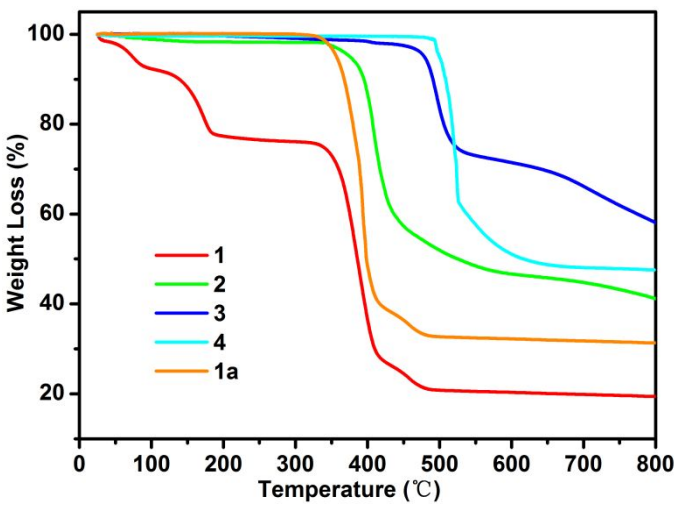

Figure S10. TGA curves for complexes **1-4** and activated sample **1a**.

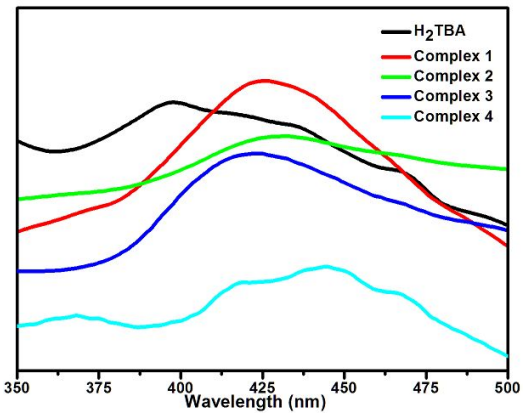

Figure S11. The fluorescence spectrum of free H_2BTA and **1**-**4**.

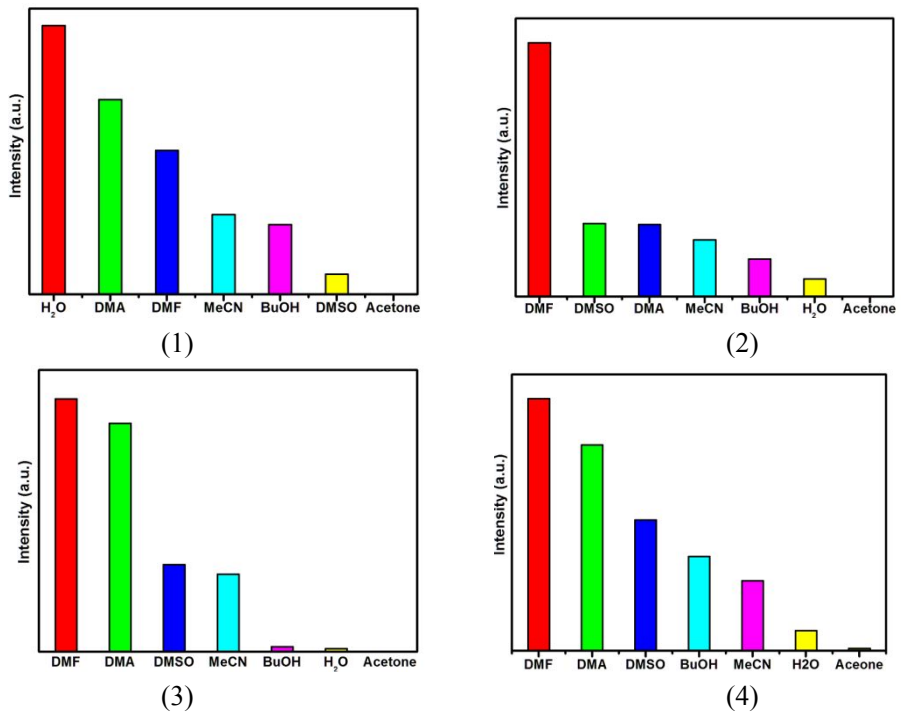

Figure S12. The luminescence intensities of complexes **1**-**4** after dispersed in different solvents.

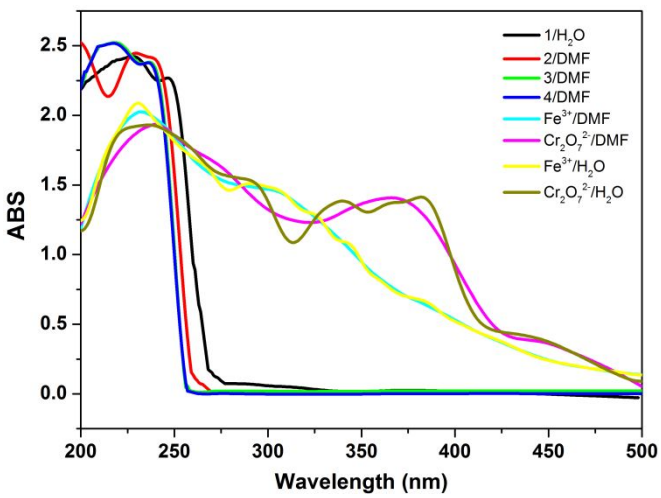

Figure S13. The UV-Vis spectrum of Fe^{3+} cation and $Cr_2O_7^{2-}$ anion and CPs **1**-**4**.

CO_2/CH_4 Selectivity Prediction via IAST

In order to compare the efficiency of **1** and **2** for CO_2/CH_4 separation, we used the IAST of Myers and prausnitz along with the pure component isotherm fits to determine the molar loadings in the mixture for specified partial pressures in the bulk gas phase [1, 2]. The measured experimental data on pure component isotherms for CO_2 and CH_4 were first converted to absolute loading using the Peng-Robinson equation of the fluid densities. The absolute component loading at 298 K were fitted with a single-site Langmuir-Freundlich model (Equation 1).

$$N = a \times \frac{bp^c}{1+bp^c} \quad (1)$$, Here, a is saturation capacity, b and c are constant.

The adsorption selectivities, S_{ads}, for binary mixtures of CO_2/CH_4, defined by (Equation 2):

$$S_{ads} = \frac{x_i / x_j}{y_i / y_j} \quad (2)$$

S_{ads}: adsorption selectivity; x_i: the mole fractions of component i in the adsorbed phases; y_i: the mole fractions of component i in the bulk phases.

Reference

(1) Myers, A. L.; Prausnitz, J. M. Thermodynamics of mixed-gas adsorption. *AIChE journal*. **1965**, *11*, 121-127.

(2) Liang, J. Y.; Li, G. P.; Gao, R. C.; Bai, N. N.; Tong, W. Q.; Hou, L.; Wang, Y. Y. Four New 3D Metal–Organic Frameworks Constructed by a V-shaped Tetracarboxylates Ligand: Selective CO_2 Sorption and Luminescent Sensing. *Cryst. Growth Des.* **2017**, *17*, 6733-6740.

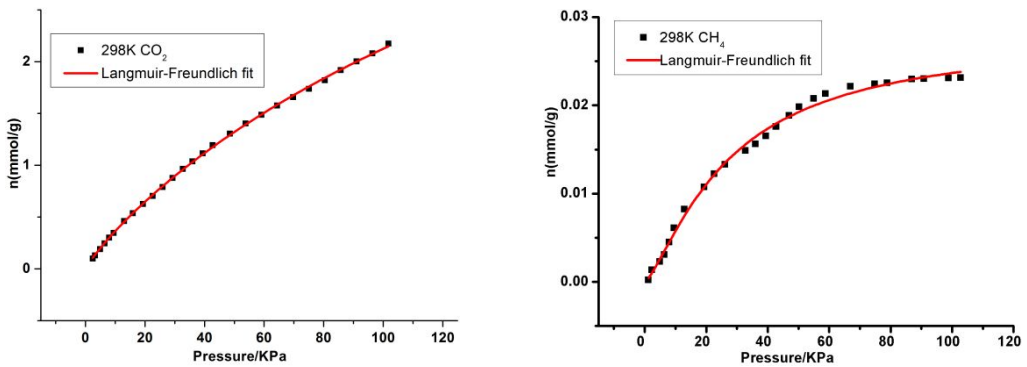

Figure S14. CO_2 adsorption isotherms of **1** at 298K with fitting by L-F model: a = 7.28924, b =0.00067, c = 0.8941, Chi^2 = 1.43408 $\times 10^{-4}$, R^2 = 0.99967; CH_4 adsorption isotherms of **1** at 298K with fitting by L-F model: a = 0.025, b = 0.00953, c = 1.46492, Chi^2 = 2.37504 $\times 10^{-6}$, R^2 = 0.97957.

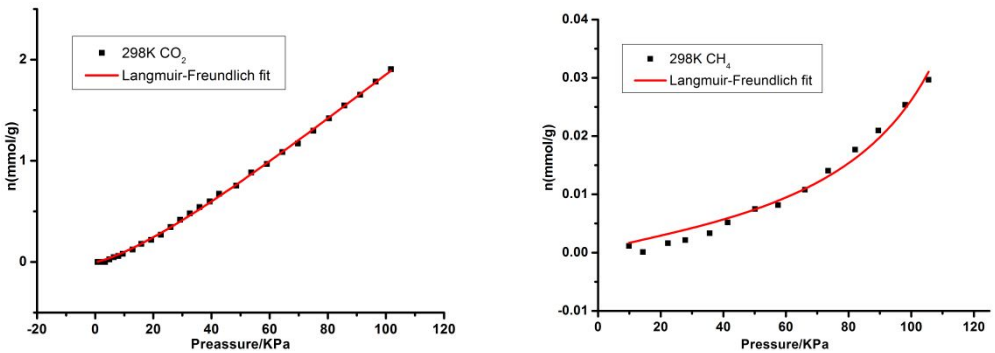

Figure S15. CO_2 adsorption isotherms of **2** at 298K with fitting by L-F model: a = 17.40921, b = 2.74954 $\times 10^{-4}$, c = 1.31826, Chi^2 = 2.39288 $\times 10^{-4}$, R^2 = 0.99936; CH_4 adsorption isotherms of **2** at 298K with fitting by L-F model: a = -0.00662, b =-0.05135, c = 0.59578, Chi^2 = 1.9989 $\times 10^{-6}$, R^2 = 0.97838.

Table S1. Crystal data for **1–4**

Compond	**1**	**2**	**3**	**4**
Frmula	$C_{20}H_{20}N_4O_7Zn$	$C_{14}H_8N_4O_4Zn$	$C_{14}H_8N_4O_4Pb$	$C_{14}H_8N_4O_4Pb$
Formula weight	493.79	361.63	503.44	503.44
Temperature/K	100	150.15	273.15	100
Space group	*P*-1	*P*-1	$P2_1/c$	C2/c
Crystal system	triclinic	triclinic	monoclinic	monoclinic
a/Å	8.3696(2)	7.2623(4)	13.8894(7)	15.1377(18)
b/Å	8.7148(3)	9.4869(6)	9.1415(5)	4.6373(7)
c/Å	15.8314(4)	13.3903(8)	10.6773(6)	20.118(2)
α/°	88.708(2)	91.557(4)	90	90
β/°	89.773(2)	93.632(4)	103.377(2)	108.315(13)
γ/°	70.011(3)	102.588(3)	90	90
V(Å^3)	1084.89(6)	897.77(9)	1318.91(12)	1340.7(3)
Z	2	2	4	4
ρ_{calc}g/cm^3	1.512	1.338	2.535	2.494
μ/mm^{-1}	1.181	1.389	12.821	12.613
F(000)	508.0	364.0	936.0	936.0
2θ range (deg)	5.654 to 52.742	5.462 to 52.732	5.38 to 55.206	5.928 to 52.704
GOF on F^2	1.049	0.996	1.105	0.958
R_{int}	0.0351	0.1022	0.0449	0.0710
Data/restraints/params	4437/144/343	3656/0/208	3042/0/208	1351/0/105
R^1, wR^2 (I>=2σ (I))[a]	0.0395, 0.1054	0.0485, 0.0920	0.0205, 0.0476	0.0421, 0.0688
R^1, wR^2 (all data)[a]	0.0482, 0.1109	0.0819, 0.1008	0.0236, 0.0488	0.0476, 0.0713
CCDC number	1852351	1852353	1852352	1852350

[a] $R_1 = \Sigma| |F_o|-|F_c| | / \Sigma|F_o|$, $wR_2 = [\Sigma w(F_o^2-F_c^2)^2] / \Sigma w(F_o^2)^2]^{1/2}$

Table S2. Selected bond lengths (Å) and angles (deg) for complex **1**.

Zn1- O1	1.9455(19)	Zn1- N2[1]	2.009(2)
Zn1- O3	1.957(2)	Zn1- N4[2]	2.028(2)
O1- Zn1- O3	106.12(9)	O1- Zn1- N2[1]	114.02(9)
O1- Zn1- N4[2]	118.75(10)	O3- Zn1- N2[1]	117.03(10)
O3- Zn1- N4[2]	95.73(9)	N2[1]- Zn1- N4[2]	104.33(10)

Symmetry codes: [1]-X, 1-Y, 1-Z; [2]-1+X, Y, +Z; [3]1-X, -Y, 1-Z; [4]1-X, 1-Y, 2-Z; [5]1-X, 1-Y, 1-Z.

Table S3. Selected bond lengths (Å) and angles (deg) for complex **2**.

Zn1- O1[1]	1.965(3)	Zn1- N2	1.991(3)
Zn1- O3	2.001(3)	Zn1- N3[2]	1.998(3)
O1[1]- Zn1- O3	104.94(12)	O1[1]- Zn1- N3[2]	117.21(11)
O1[1] -Zn1- N2	99.35(11)	N2- Zn1- O3	109.83(12)
N2- Zn1- N3[2]	123.27(13)	N3[2]- Zn1- O3	101.14(11)

Symmetry codes: [1]-X, 1-Y, -Z; [2] -1+X, Y, Z; [3]1-X, 2-Y, -Z; [4]-X, 1-Y, -1-Z.

Table S4. Selected bond lengths (Å) and angles (deg) for complex **3**.

Pb1- O1[1]	2.560(3)	O1- Pb1[4]	2.560(3)
Pb1- O2[1]	2.881(4)	O2- Pb1[4]	2.881(4)
Pb1- O3[2]	2.462(3)	O3- Pb1[2]	2.462(3)
Pb1- O4[3]	2.700(3)	O4- Pb1[5]	2.700(3)
Pb1- N1	2.497(4)	Pb1- N3	2.402(3)
O1[1]- Pb1- O2[1]	47.52(10)	O3[3]- Pb1- O4[2]	86.70(9)
O1[1]- Pb1- O4[2]	113.66(10)	O3[3]- Pb1- N1	84.91(12)
O3[3]- Pb1- O1[1]	153.10(10)	O4[2]- Pb1- O2[1]	66.15(9)

O3[3]- Pb1- O2[1]	148.26(10)	N1- Pb1- O1[1]	76.04(11)
N3- Pb1- O1[1]	80.26(11)	N1- Pb1- O2[1]	123.43(11)
N3- Pb1- O3[3]	77.94(9)	N1- Pb1- O4[2]	169.99(10)
N3- Pb1- N1	80.38(12)	N3- Pb1- O2[1]	92.01(10)
N3- Pb1- O4[2]	103.17(10)		

Symmetry codes: [1]X, Y, 1+Z; [2]1-X, 1-Y, 1-Z; [3]1-X, 1/2+Y, 1/2-Z; [4]2-X, 1-Y, 2-Z; [5]1-X, 2-Y, 1-Z.

Table S5. Selected bond lengths (Å) and angles (deg) for complex **4**.

Pb1- O1	2.409(6)	Pb1- O1[1]	2.409(6)
Pb1- O2[2]	2.731(6)	Pb1- O2[3]	2.731(6)
Pb1- N2[4]	2.619(6)	Pb1- N2[5]	2.619(6)
O1- Pb1- O1[1]	93.1(3)	O1[1]- Pb1- O2[2]	145.39(16)
O1[1]- Pb1- O2[3]	82.1(2)	O1- Pb1- O2[2]	82.1(2)
O1- Pb1- O2[3]	145.39(16)	O1- Pb1- N2[4]	85.48(19)
O1[1]- Pb1- N2[5]	85.48(19)	O1- Pb1- N2[5]	73.65(17)
O1[1]- Pb1- N2[4]	73.66(17)	O2[3]- Pb1- O2[2]	120.2(3)
N2[5]- Pb1- O2[3]	71.80(19)	N2[4]- Pb1- O2[3]	125.00(19)
N2[5]- Pb1- O2[2]	125.00(19)	N2[4]- Pb1- O2[2]	71.80(18)
N2[4]- Pb1- N2[5]	149.6(3)		

Symmetry codes: [1]1-X, +Y, 3/2-Z; [2]X, 1+Y, Z; [3]1-X, 1+Y, 3/2-Z; [4]1/2+X, 1/2+Y, Z; [5]1/2-X, 1/2+Y, 3/2-Z; [6]X, -1+Y, Z; [7]-1/2+X, -1/2+Y, Z; [8]1/2-X, 3/2-Y, 1-Z.

ICP measurements:

After the fluorescence experiment, the suspension was filtered. And filter cake (CPs) was washed with fresh solvent for several times. Then, ICP measurements were performed on the filtrate (solution containing Fe^{3+} ions), filter cake (CPs) and as-synthesize samples (CPs). The results are as following (Table S6 and Table S7):

Table S6. The amounts of Zn^{2+}/Pb^{2+} and Fe^{3+} ions in filter cake after washing treatment

Compound	Zn^{2+} (wt%)	Fe^{3+} (wt%)	Compound	Pb^{2+} (wt%)	Fe^{3+} (wt%)
1[a]	12.92	-	**3**[a]	41.12	-
1[b]	12.86	0.11	**3**[b]	41.00	0.08
2[a]	18.09	-	**4**[a]	40.92	-
2[b]	18.03	0.09	**4**[b]	40.82	0.06

[a]: as-synthesize samples (CPs); [b]:CPs after the fluorescence experiment.

Table S7. The concentration of Fe^{3+} ($mol \cdot L^{-1}$)

CPs	**1**	**2**	**3**	**4**
The initial concentration of Fe^{3+}	1.0×10^{-2}			
The concentration of Fe^{3+} in filtrate after sensing measurement	0.9980×10^{-2}	0.9983×10^{-2}	0.9985×10^{-2}	0.9989×10^{-2}

As can be seen from Table S6 and Table S7 that the amount of Zn/Pb elements in filter cake were much larger than that of Fe, and the concentration of Fe^{3+} was basically the same before and after the fluorescence experiment, which indicate that the observed quenching effect should not arise from an ion-exchange process.